Research Article

Tianyu Yu, Wenfeng Guo, Xinjian Wang, Junyan Liu*, Yang Wang*, and Mingjun Chen

Surface hydrophobicity and oleophilicity of hierarchical metal structures fabricated using ink-based selective laser melting of micro/nanoparticles

https://doi.org/10.1515/ntrev-2020-0050
received May 23, 2020; accepted June 22, 2020

Abstract: Hierarchical structures have attracted considerable interest due to their super-oleophobic/super-hydrophobic behavior. However, it is rare to present a novel additive manufacturing (AM) approach to fabricate hierarchical metal structures (HMSs). A micro/nano mixture ink was deposited on a substrate and a laser was used to selectively scan the ink layer. A new layer of ink was deposited on the previous consolidation layer during manufacturing. The surfaces of the as-sintered HMSs exhibit inherently super-hydrophilic and super-oleophobic behavior with a 155° contact angle (CA) with oil. Furthermore, the HMSs were successfully turned into super-hydrophobic and super-oleophilic mode (with a 152° CA) after surface modification with a solvent-free, electrostatic polytetrafluoroethylene particle deposition. They can be used as oil/water separation media by the functional surfaces existing in the pore channels. The experimental study of HMSs shows an effective removal of oil contaminants from water. The developed process also possesses an advantage of AM of HMSs with complex shapes in ambient air under the protection of an organic ink. Importantly, the present approach could be extended to a vast number of HMSs, for the preparation of highly durable functional materials for various applications.

Keywords: super-hydrophobicity, super-oleophilicity, selective laser melting, additive manufacturing, hierarchical metal structures

1 Introduction

Oil contamination is a critical issue that impacts the global environment. For the cleaning of oily wastewater generated in remote and extreme conditions, high performance devices have to be developed for the oil/water separation. A superhydrophobic bulk substrate could be a sound choice due to its light weight, robustness, high strength, and corrosion resistance. The surface properties of such components are critical to their performance. Nanostructures fabricated using nanowires, nanotubes, nanobeams, nanoplates, graphene sheets, and nanoshells could provide unique capabilities for nano-sensors, probes, and surface functionalities [1]. Surface functionalities such as super-hydrophobicity is an interfacial property with a water contact angle (CA) greater than 150°, enabling many applications in industrial and biomedical processes [2–6]. The superwettable property can be used for contaminated oil recovery [7]. In order to achieve a super-hydrophobic surface, usually a low surface energy and a micro/nano hierarchical microstructure are needed [5]. Super-hydrophobicity has been enabled and attracted considerable interest due to its potential of separating oils/organic pollutants from marine ecosystems [8–10]. A highly efficient metal–organic framework (MOF)/carbon nanotube (CN) foam with micrometer-sized pores of CNs for the efficient conversion of CO_2 into cyclic carbonates was fabricated for water/oil separation. The MOF crystals attached on the foam surfaces created a natural shield against water [11]. A NiCrN hydrophobic coating was prepared and deposited on steel and silicon wafer substrates using multi-arc ion plating by Du et al. [12]. With the increase of deposition temperature, the surface morphology changed to a micro-nano hierarchical structure with a CA of over 140°. The adsorption of hydrocarbons on the coated surface presented a unique self-repair capability after wear. Janus particles were used to form aggregates with

* **Corresponding author: Junyan Liu,** State Key Laboratory of Robotics and System, Harbin Institute of Technology, Harbin, Heilongjiang, 150001, China; School of Mechatronics Engineering, Harbin Institute of Technology, Harbin, Heilongjiang, 150001, China, e-mail: ljywlj@hit.edu.cn
* **Corresponding author: Yang Wang,** State Key Laboratory of Robotics and System, Harbin Institute of Technology, Harbin, Heilongjiang, 150001, China; School of Mechatronics Engineering, Harbin Institute of Technology, Harbin, Heilongjiang, 150001, China, e-mail: wyyh@hit.edu.cn
Tianyu Yu, Wenfeng Guo, Xinjian Wang, Mingjun Chen: State Key Laboratory of Robotics and System, Harbin Institute of Technology, Harbin, Heilongjiang, 150001, China; School of Mechatronics Engineering, Harbin Institute of Technology, Harbin, Heilongjiang, 150001, China

hierarchical structures, ranging from the nanometer-scale up to hundreds of micrometers, which exhibited ultra-hydrophobic behavior [13]. Porous conducting polymers were synthesized on carbon fiber cloth by electrochemical polymerization of pyrrole with bipyrrole and doping of the polymer with surfactant anions, showing superhydrophobic behavior [14]. Chen et al. [15] synthesized 3D interconnected porous CN/copper composites using pre-compression, chemical vapor deposition, and spark plasma sintering. The composites show excellent strength and corrosion resistance, maintaining good conductivity. Wang et al. [16] developed 3D hollow quasi-graphite capsules/polyaniline hierarchical composites by decorating protonated polyaniline on the surface of graphite capsules. The nanospheres decorated on the inner and outer surfaces of the graphite capsules provide a large surface area for NH_3 gas adsorption, and a potential gas sensor application was developed. Jian et al. [17] developed a $ZrN_{0.4}B_{0.6}$/SiC nanocomposite using chemical vapor deposition and chemical vapor infiltration. The nanohybrid structures interconnected with the nanofiber network enhance the interfacial area, thus enhancing the microwave absorption. Guo et al. [18] developed an FeSiAl core with an oxidation gradient ceramic coating composite through a multi-medium plasma method. Due to strong synergistic magnetic–dielectric effects, the multistrata core–shell composites show excellent microwave absorption capability and high temperature oxidation resistance. Sorbent materials, such as polyurethane [19], polyvinyl-alcohol formaldehyde [20], poly aerogel [21], carbon soot [22], and graphene/polymer aerogels, are considered as promising media for oil/water separation [23]. A porous sorbent material usually requires further treatment such as immobilization of nano-scaled particles on the surface to achieve hydrophobicity. However, some of the materials or reagents used in the fabrication process are environmentally unfriendly, and their manufacturing processes are time consuming or have part size limitation such as tens of micrometers thick thin films [24].

Additive manufacturing (AM) refers to a rapid prototyping technique that uses a layer-by-layer approach to fabricate digital CAD models [25,26]. The selective laser melting (SLM) [27] technique has been used to manufacture a variety of materials such as stainless steel [28,29], aluminum [30,31], and nickel- and titanium-based alloys with relatively high resolution and geometric accuracy compared with other AM techniques [32–35]. SLM also enables the fabrication of lightweight cellular lattices or porous structures that are difficult to manufacture with other AM techniques due to the support from the powder bed [36–38]. SLM generally requires a vacuum or inert gas protected environment to avoid the oxidization of sintered materials, which increases the operation costs and decreases its feasibility. However, an ink-based solution can act as the protection environment during laser–matter interaction due to the absence of material oxidation problems. Guo et al. [39] studied the fabrication of hierarchical composites using Inconel 718 micro-powder with irregular-shaped nano-sized TiC particles. The effect of laser scan speed on the surface wettability and corrosion resistance was studied, and the water CA reached ~151.5° for a laser scan speed of 600 mm/s. Kang et al. [40] fabricated hierarchical composites using SLM of nickel-coated high-silicon steel powder. Anisotropic magnetic properties were found due to the rod-shaped structure, and the magnetization saturation presents a negative correlation with laser scanning speed. Arakane et al. fabricated Cu-rich and Cu_2O-rich microheaters using femtosecond laser-induced reduction of CuO nanoparticles [41]. An array copper layer with reduced friction was fabricated by using SLM of Cu nanoparticle-based organic inks, showing the capability of ink-based SLM (ISLM) for surface micro-texturing [37], and this technique was also used to fabricate a nano-scaled amorphous carbon-coated Cu layer with super-hydrophobic behavior by decomposing the polymer in the solvent [42], showing that ISLM is a potential technique to fabricate functional structures. A multilayered organic–inorganic columnar structure was fabricated by Wei et al. by sequentially assembling rutile titanium dioxide nanorods, polymers, and graphene oxide in a layer-by-layer fashion to form an organic–inorganic structure [43]. The mechanical properties are comparable to those of natural enamel.

It is of great significance to develop an efficient and effective method to fabricate hierarchical metal structures (HMSs) with complex geometries and hierarchical structures in one step. The flexibility and robustness of AM methods provide a solid tool to enable fabrication of such structures with superior surface functionality. In this work, a novel ink-based AM technique was developed (Figure 1).

A micro/nanoparticle-based organic ink was deposited layer by layer during an SLM process to fabricate HMSs in ambient air. The organic solvent prevents the oxidation during the ISLM process where Cu-NPs covered the surfaces of stainless steel micro particles (SS-MPs) due to the surface tension difference among the melt, surrounding Cu-NPs and organic solvent. Due to the laser-induced self-assembly behavior, Cu-NP-shelled HMSs with a hierarchical structure were successfully

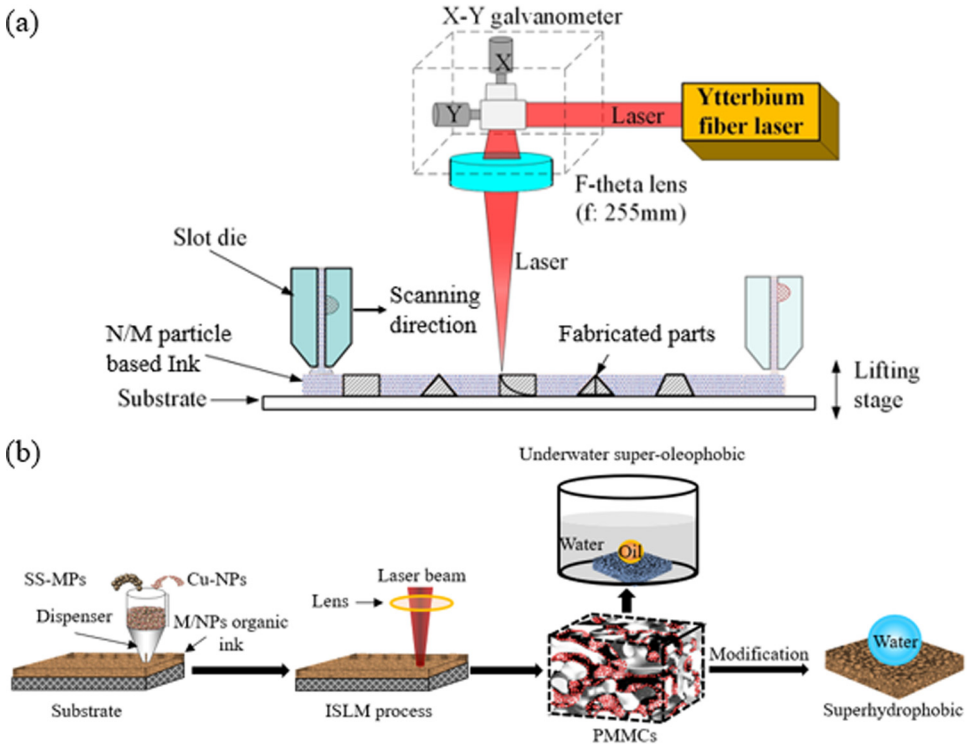

Figure 1: (a) Schematic of the ISLM framework of hierarchical metal composites consisting of ink deposition, laser scanning, as-built oleophobicity, and surface modified super-hydrophobicity and super-oleophilicity; (b) schematic of the ISLM process consisting of a single moving laser beam, an organic solvent with micro/nanoparticles, built parts and a substrate.

fabricated in ambient air in a single step. Furthermore, the HMSs were successfully switched to super-hydrophobic and super-oleophilic mode after surface modification by using a solvent-free, electrostatic polytetrafluoroethylene particle deposition technique. The water/oil CAs were measured to analyze the surface hydrophobicity and oleophobicity. Both static and dynamic oil/water mixture separation experiments were conducted. In addition, the surface morphology and microstructure of the particles and HMSs were characterized using a scanning electron microscope (SEM) and X-ray diffraction (XRD). Durability tests of the HMS surface functionality in the pH range of 1–13 were conducted as well.

2 Experimental section

2.1 Materials

Cu-NPs (Guangzhou Hong Wu Material Technology Co., Ltd, China) with a size of 70–100 nm and 316L SS-MPs (HLPOWDER, Changsha Hualiu Powder Metallurgy Co., Ltd, China) with a size range of 10–38 μm were used in this work. Oils of *n*-heptane and trichloromethane (TCM) served as organic oils for the oil/water separation tests. Polyvinylpyrrolidone (PVP, MW = 10,000) was adopted to stabilize the NPs in the solvent mixture. 1*H*,1*H*,2*H*,2*H*-Perfluoro-decyl-triethoxysilane (PFDTS; Sigma-Aldrich Co. LLC, USA) was utilized for the surface modification. ANSI 304 stainless steel plates with a thickness of 2 mm were cleaned three times in an ultrasonic bath with an ethanol/water (1:1) solution for 5 min before being used as substrates.

2.2 ISLM process

In order to obtain the solvent mixture of micro/nanoparticles, organic solvents PVP (8.19 wt%) and ethylene glycol (27.4 wt%) were prepared to prevent the agglomeration and oxidation of Cu during SLM. The Cu-NPs (17.56 wt%) were dispersed in the mixed organic solvent and stirred with ultrasonic waves for 25 min. Then, the ANSI 316L SS-MPs (46.85 wt%) were added in the solvent mixture and homogenized using ultrasonic waves for another 15 min.

One of the typical methods of SLM is to use a mixture of two functional materials which contains a structural material and a binder material with a lower melting point to stabilize the structural material [44]. The binder material can fill up the micro-pores and create a high capillary force for rearrangement of the structural particles [45]. Our previous work illustrates that this method can fabricate a pure copper layer in ambient air [46]. This motivates us to use Cu-NPs as a binder material in SLM of SS-MPs in ambient air, fabricating hierarchical and surface functional composites. In this ISLM process, a fiber laser was used to heat the solution with the mixture of ANSI 316L MPs and Cu-NPs. Thus, pure copper could be formed under the protection of a reduction solvent. Furthermore, under the irradiation of the laser, SS-MPs and Cu-NPs will simultaneously melt and react with the surrounding chemicals.

A continuous ytterbium fiber near-infrared laser (wavelength of 1,070 nm) with a fast scanning optical system (focal length ~255 mm) was developed for the ISLM process. The experimental setup is illustrated in Figure 1b. An optimized slot die was designed and applied to deposit the organic solvent mixture. The layer thickness of the solvent layer was kept as 40 μm. Each newly deposited solvent layer is kept at 70°C through a radiation heater, and the layer deposition time is 0.5 s. A laser power of 25 W, a laser spot size of 18 μm, a scan speed of 35 mm/s, and a hatch space of 0.1 mm were used for fabricating the HMS samples. After the first layer of the organic solvent was deposited and sintered, another layer would be spread on the previous sintered layer, and this process was repeated until a solid HMS part was fabricated, and the 3D parts were manufactured with a slicing space of 0.04 mm.

2.3 Characterization

SEM tests were performed on a field-emission SEM (FEI Helios Nanolab 600i). Powder XRD patterns were recorded using a D/MAX-RB diffractometer (RIGAKU Corporation, Japan) with Cu Kα radiation. EDS mapping data were obtained by using an AZtecEnergy Standard X-MaxN 50 instrument (Oxford Instruments). X-ray photoelectron spectroscopy (XPS) data were measured using an ESCALAB 250Xi instrument (ThermoFisher, USA). The CA was measured by using a CA system (OCA20; Data Physics, Germany) using a droplet (3 μL) of water or oil as an indicator. For in-water CA measurements, the HMS samples were first fully immersed in water, and a droplet (3 μL) of TCM was carefully dropped on its surface. Three measurements of each CA test were conducted, and the average value was recorded. The surfaces of the fabricated HMS samples were then modified to decrease their surface energy by immersing them in an ethanol solution (1 wt%) of PFDTS at a temperature of 40°C for 24 h, followed by washing with ethanol and drying at 130°C for 1 h. Water CA tests using the modified HMS samples were then conducted. The pH durability test was conducted by immersing the samples in an aqueous HCl or NaOH solution with a pH range of 1–13 for 12 h, and then the CA tests were carried out on the dried samples.

3 Results and discussion

3.1 Morphological and XRD analyses of the HMS samples

The composition of Cu-NPs only fabricated using ISLM was characterized (Figure S1, Supplementary material). The dynamic formation of the Cu-shelled-SS hierarchical structure during the ISLM process is very complex, due to the existence of ethylene glycol and differences of specific weight, surface tension, solidification rate between stainless steel and copper. The absorptivity of copper for the near-infrared laser radiation is much lower than that of iron. When copper and stainless steel were exposed to the same laser irradiation conditions, the heating rate of stainless steel would be higher than that of copper. Since the melting point of Cu-NPs is lower than that of SS-MPs, they would melt almost simultaneously under a high laser power intensity. During the ISLM process, the solvent was heated as well. Ethylene glycol near the top of the ink would evaporate, which leads to a faster cooling rate. The SS-MPs and Cu-NPs in the ethylene glycol solvent would be protected during laser irradiation from oxidation. Additionally, the oxidized of Cu-NPs can be further suppressed by their reaction with ethylene glycol.

Figure 2a shows a coral-like structure of an HMS sample surface. The formation of the hierarchical structures was attributed to the fusion of aggregates. The open pores were formed from the space trapped within the loose SS-MPs. The result from XRD is presented in Figure 2b, indicating that pure copper was formed during the ISLM process. However, based on the observation, the black color of the sintered composites

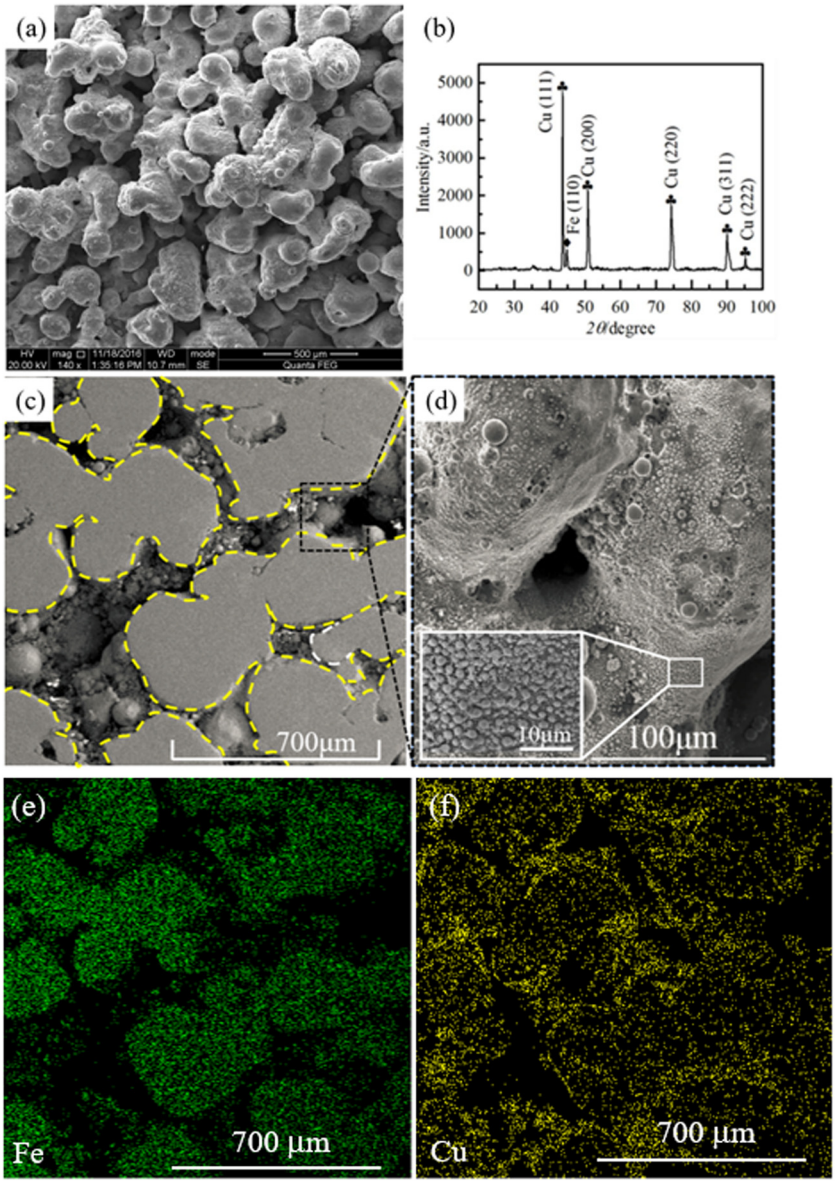

Figure 2: (a) Surface morphology of the HMS sample investigated using an SEM; (b) XRD results of the HMS sample. (c and d) SEM images showing the surface morphology of the sintered HMS sample with a unique micro/nano hierarchical structure. (e and f) Energy-dispersive spectroscopy elemental mapping of the as-sintered HMS sample for Fe and Cu atoms.

indicates that some of the materials on the surface are oxidized to CuO. The XRD tests possess a specific depth of penetration where the CuO formation on the surface has not been detected, which further implied that only a very thin layer of CuO was formed due to the evaporation of the reduction solvent on each layer surface. In the meantime, the organic solvent in the adjacent areas would enter the laser irradiation region through the capillary effect, and the CuO would be deoxidized into Cu due to the reaction with the organic solvent. Some of the CuO on the top surface of each layer would be saturated by the next layer of ink and turned into Cu as a result.

Figure 2c shows the surface morphology of the HMS sample. A detailed micro-graph is shown in Figure 2d. It can be observed that due to the surface tension and wettability, a nano-size copper structure would uniformly cover the surface of HMS samples, which shows self-assembly behavior. This autonomous organization of Cu-NPs into patterns or structures is further investigated in the next section for its wetting behavior. Energy dispersive X-ray spectroscopy mapping of Fe and Cu on the as-sintered HMS sample illustrated the growth of the Cu-NPs over the entire HMS surface after the ISLM process (Figure 2e and f).

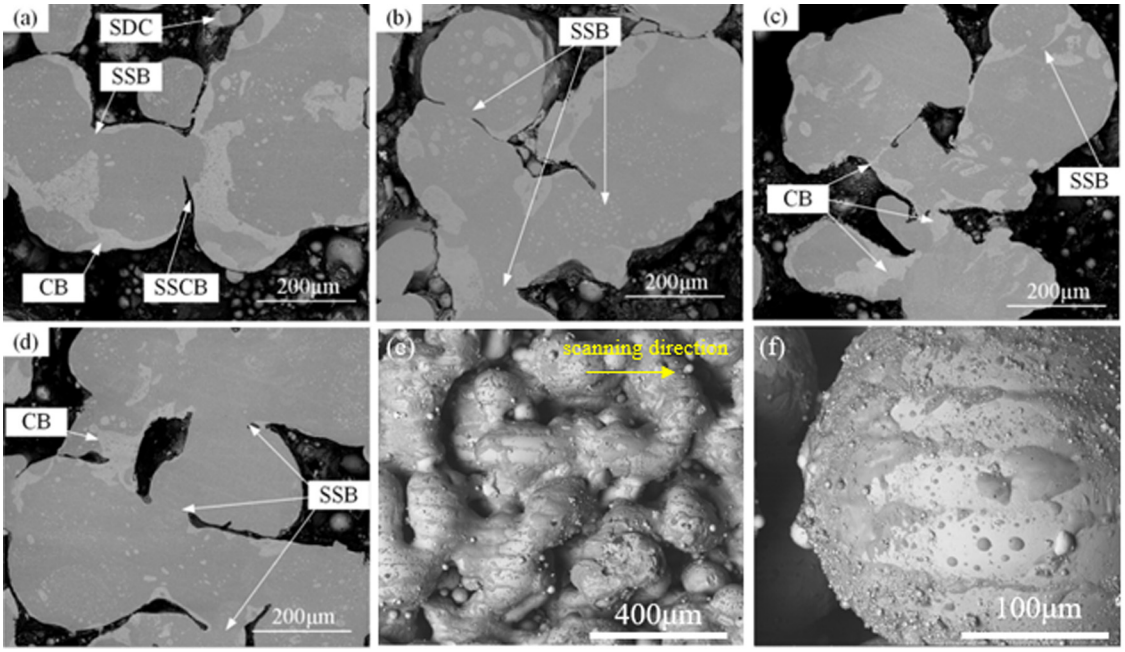

Figure 3: (a–d) Cross-section SEM images of the HMS samples showing the morphology after sintering such as SDC, SSB aggregates, CB aggregates, and SSCB. (e and f) The morphology of the HMS structure showing a clear Cu-NP melt pattern along the laser scanning direction.

Small amounts of CuO and Cu_2O as well as carbides were found on the surfaces of Cu-NPs using XRD and XPS analysis. Figure 3 shows a typical cross-section morphology of the cut HMS samples obtained using SEM secondary electron mode, in which the steel shows a darker color and the copper shows a lighter color. The compositions of both were characterized by using EDS (Figure S2, Supplementary material). It can be seen in Figure 3 that during the sintering process, alloying of the SS-MPs and Cu-NPs occurred, and the copper layers were covered on the stainless steel agglomerates (lighter color on the boundaries). Further agglomeration/bridging occurred among these aggregates and formed the closed micro-pores. Full melting of the powders due to the laser irradiation can be observed.

During sintering, the interaction among aggregates was non-uniform and different bridging behaviors were found. Four different alloy regions can be observed in Figure 3a–d. The first type is the separately distributed copper (SDC). SDC covered isolated stainless steel melt without interrupting the surrounding materials. The second type is the stainless steel bonded (SSB) aggregate. The successive heating by laser irradiation connects the melt of stainless steel along the scan path, which results in fusion among the adjacent stainless steel aggregates. The third type is the copper bonded (CB) aggregate. Since the Cu-NPs are uniformly adhered around the SS-MPs, the copper melt could finally result in the fusion among other Cu-NPs. The last type is the aggregate fused by stainless steel and copper bonding (SSCB), which resulted from the melt copper being drawn inside the adjacent stainless steel and forming a close bond with another aggregate. By the combination of these four types of fusion, the Cu-shelled-SS hierarchical structure of the HMSs was formed. The morphology of the HMS structure showed a clear Cu-NP melt pattern along the laser scanning direction (Figure 3e and f and Figure S3, Supplementary material).

3.2 Wetting behavior and oil/water separation capability of HMS samples

In order to examine the wetting behavior of the as-built HMS samples with water and oil, an in-water CA experiment was carried out. Figure 4a shows the in-water CA test with TCM, and Figure 4b presents the in-water wetting behavior with Oil-Red O dyed TCM. A nearly 0° water CA and ~155° in-water oil CA were obtained, indicating its super-hydrophilic and in-water super-oleophobic functionalities. These functionalities are attributed to the micro/nano hierarchical structures formed by the Cu-NP self-assembly phenomenon during the ISLM process. The hydrophilic behavior of the HMS structure resulted from the high surface energy and capability of wetting the

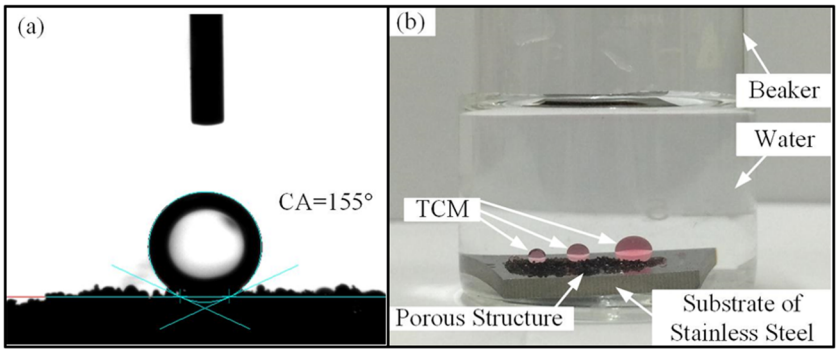

Figure 4: In-water super-oleophobic and hydrophilic behavior of the HMS sample showing a 155° CA with Oil-Red O dyed TCM and a nearly 0° water CA; (a) in-water CA measurement with TCM; (b) tests with the in-water TCM (Oil-Red O dyed) showing the super-oleophobic capability.

surfaces. When an HMS sample was immersed in water, the structure would be fully infiltrated, which forms a water membrane at the boundaries.

For the purpose of investigating the wetting ability of the HMS material, the fabricated samples were surface modified to decrease the surface energy by immersing the samples in an ethanol solution of PFDTS. The surface morphology after the modification can be found in Figure S4, Supplementary material. The wetting behavior of the modified samples is shown in Figure 5a, and a 152° CA with water and a nearly 0° oil CA were found. The wetting behavior was completely switched after surface modification. This demonstrated that the ISLM-fabricated HMS samples could switch from super-hydrophilicity to super-hydrophobicity by suitable surface modification.

Furthermore, based on the surface functionality changes, the HMS samples were tested for their oil collection capability from water as shown in Figure 5. Oils of *n*-heptane and TCM were selected as the organic oils to test the super-oleophilicity of the modified HMS sample. Figures 5b–d show the process of separating TCM (Oil-Red O dyed) from water. The water was repelled from the sample surface, which allows the sample to collect the majority of the oil in the water surface. Figure 5e–h shows the process of separating *n*-heptane (dyed orange) on the

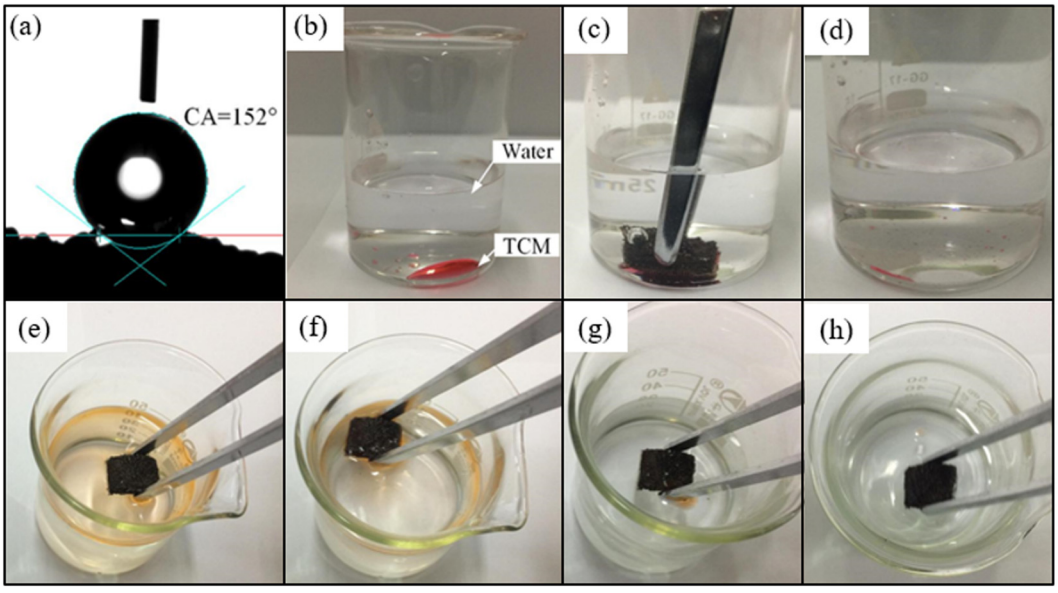

Figure 5: (a) Water CA test of the HMS sample after surface modification showing a 152° CA with water and a nearly 0° oil CA; (b–d) the process of separating TCM (Oil-Red O dyed) from water; (e–h) the process of separating *n*-heptane (dyed orange) from water; the unique hierarchical structure of the HMS sample shows its superior performance for oil/water separation under both in-water and on-the-surface-of-water conditions.

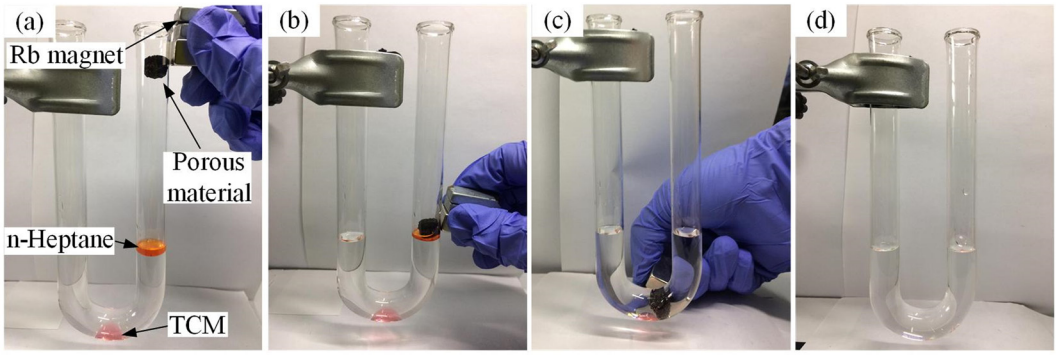

Figure 6: Oil/water separation tests of the HMS sample in a curved glass tube under the actuation of a permanent magnet. (a) HMS sample driven by a permanent magnet; (b) HMS sample absorbed *n*-Heptane completely; (c–d) HMS sample absorbed TCM completely and left a clear glass tube.

surface of water; the *n*-heptane was completely removed from water by the HMS sample. The collected oil can be removed from the samples afterward through nitrogen gas cleaning. The unique hierarchical structure of the HMS sample shows its superior performance for oil/water separation under both in-water and on-the-surface-of-water conditions.

The magnetic actuation behavior of the HMS samples was also investigated. Figure 6 shows that the fabricated HMS sample moves under the control of a permanent magnet. The oil/water separation experiment was conducted in a curved glass tube. A surface modified cylindrical HMS sample with a diameter of 12 mm and a height of 6 mm is fabricated for the test. A total of 300 µL *n*-heptane and 300 µL TCM are dripped into the tube slightly. Four times collection were conducted to separate the oil from water thoroughly, as shown in Figure 6. The HMS material fabricated using the ISLM technique shows a promising performance in oil/water separation with its super-oleophilicity.

A test apparatus was also made to test the flowing/dynamic oil/water separation capability of the fabricated HMS samples. An HMS sample with a thickness of 0.5 mm was sintered and covered on an acrylic tube. A mixture of water and *n*-heptane was prepared and put into the acrylic tube with a small inclination that allows the liquid to flow through the porous sample as shown in Figure 7a. Due to the super-oleophilicity and super-hydrophobicity of the HMS sample after the surface modification, the *n*-heptane flowed through the sample completely.

3.3 Durability tests of the HMS surface functionality

The durability of surface functionalities such as super-oleophobicity and surface-modified super-oleophilicity of the ISLM fabricated HMS samples was investigated. The fabricated samples were all cleaned in an ultrasonic bath for 1 h to wash away the unmelt particles after being manufactured. The samples showed a stable behavior that endures through in the presence of acid or alkali. Although a few surface scales of CuO have been observed in the presence of an acid solution, the surface structures still demonstrated an excellent performance of in-water oil CA as shown in Figure 7c. The HMS sample surfaces maintain an in-water oil CA above 150° after being immersed in an aqueous HCl or NaOH solution in the pH range of 1–13 for 12 h. After surface modification, the HMS samples were treated in the aqueous HCl or NaOH solution in the pH range of 1–13 for 12 h as well. The water CA of the surface-modified samples is shown in Figure 7d, indicating the excellent acid and alkali resistance as expected. In all, the prepared samples demonstrate a strong durability and robustness under acid or alkali conditions.

3.4 ISLM of HMS samples with complex geometries

The ISLM technique developed in this study shows an advantage of fabricating micro/nano hierarchical structures that can switch from in-water super-oleophobicity to super-hydrophobicity and super-oleophilicity after appropriate surface-modification. In the ISLM process, the laser scans and sinters the M/N particle solvent mixture layer by layer under the control of X–Y galvanometers. In order to demonstrate the capability of the developed ISLM process to fabricate HMS samples with complex geometries, several different CAD models were designed. Figure 7b shows the fabricated 3D parts with a dimension of about 5 mm using the ISLM method with various shapes such as cylinder, cone, tetrahedron, and

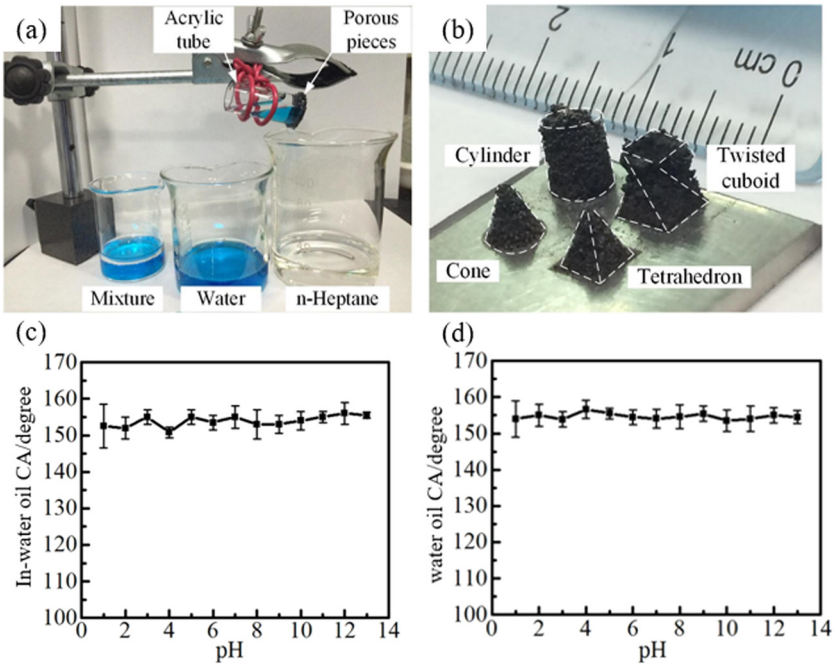

Figure 7: (a) Flowing/dynamic oil/water separation tests showing a complete oil/water separation with no water passing through the HMS sample (water is dyed blue for illustration purpose). (b) Various structures of HMS samples that have been manufactured by ISLM techniques. (c) In-water CA of the HMSs after being immersed in aqueous solutions of various pH 1–13 for 12 h; (d) water CA of the surface modified samples after being immersed in aqueous solutions of various pH 1–13 for 12 h.

twisted cuboid, respectively. It can be seen that the ISLM technique was successfully applied for the fabrication of complex geometries of HMSs. These findings shed light on the application of HMSs in the field of bio-engineering, sensors, fluid flow control, water purification, and so forth [47]. By adjusting the contents of micro/nanoparticles as well as the organics, the ISLM technique provides a tool for customized hierarchical structure fabrication in a single step without any requirement for post-processing. Importantly, the present approach could be extended to a vast number of HMS structures, by adjusting the materials and concentration of NPs and MPs, for the preparation of highly functional materials for various applications.

4 Conclusions

In this work, we demonstrated a novel method using ISLM of stainless steel micro-particles and copper nanoparticles to fabricate micro/nano hierarchical metal composites in ambient air. The major findings are listed as follows:

(1) The hierarchical structures of the fabricated composites were formed by the connection of micro/nanoparticle aggregates with an outer shell of copper. Due to a high surface energy of the as-sintered surfaces, they showed super-hydrophilic behavior with a nearly zero water CA, expressing a good in-water super-oleophobicity with an oil CA of about 155°.

(2) The HMSs were successfully turned into super-hydrophobic/super-oleophilic mode after surface modification by using a solvent-free, electrostatic polytetrafluoroethylene particle deposition method. The surfaces showed a water CA of 152° and a nearly zero oil CA, which allows the composite samples to collect oil from water even through a curved tube using magnetic actuation.

(3) Pure copper was formed during the ISLM process due to deoxidization. Part of the composite surfaces was oxidized to CuO. The XRD tests showed that a very thin layer of CuO was formed due to the evaporation of the reduction solvent. The CuO would be deoxidized into copper due to the reaction with the organic solvent.

(4) By using the ISLM technique, hierarchical metal composite parts with complex shapes were successfully fabricated. Both static and flowing oil/water separation tests showed excellent super-hydrophobic and super-oleophilic behavior of the surface-modified hierarchical metal composite samples.

Acknowledgments: This work was supported by the Foundation for Innovative Research Groups of the National Natural Science Foundation of China under grant no. 51521003, the Chinese National Natural Science Foundation under grant no. 61571153, 51173034, Self-Planned Task (No. SKLRS202002C) of State Key Laboratory of Robotics and System (HIT), Programme of Introducing Talents of Discipline of Universities (grant no. B07108), and Application Technology Research and Development Program of Heilongjiang Province under grant no. GA19A401.

Conflict of interest: The authors declare no conflict of interest regarding the publication of this paper.

References

[1] Chandel VS, Wang G, Talha M. Advances in modelling and analysis of nano structures: a review. Nanotechnol Rev. 2020;9(1):230–58.
[2] Zhao X, Su Y, Liu Y, Li Y, Jiang Z. Free-standing graphene oxide-palygorskite nanohybrid membrane for oil/water separation. ACS Appl Mater Interfaces. 2016;8(12):8247–56.
[3] Xu L, Karunakaran RG, Guo J, Yang S. Transparent, superhydrophobic surfaces from one-step spin coating of hydrophobic nanoparticles. ACS Appl Mater Interfaces. 2012;4(2):1118–25.
[4] Liu X, Ge L, Li W, Wang X, Li F. Layered double hydroxide functionalized textile for effective oil/water separation and selective oil adsorption. ACS Appl Mater Interfaces. 2014;7(1):791–800.
[5] Deng D, Prendergast DP, MacFarlane J, Bagatin R, Stellacci F, Gschwend PM. Hydrophobic meshes for oil spill recovery devices. ACS Appl Mater Interfaces. 2013;5(3):774–81.
[6] Deng X, Mammen L, Butt HJ, Vollmer D. Candle soot as a template for a transparent robust superamphiphobic coating. Science. 2012;335(6064):67–70.
[7] Liu L, Pan Y, Bhushan B, Zhao X. Mechanochemical robust, magnetic-driven, superhydrophobic 3D porous materials for contaminated oil recovery. J Colloid Interface Sci. 2019;538:25–33.
[8] Wu J, Wang N, Wang L, Dong H, Zhao Y, Jiang L. Electrospun porous structure fibrous film with high oil adsorption capacity. ACS Appl Mater Interfaces. 2012;4(6):3207–12.
[9] Zhang A, Chen M, Du C, Guo H, Bai H, Li L. Poly (dimethylsiloxane) oil absorbent with a three-dimensionally interconnected porous structure and swellable skeleton. ACS Appl Mater Interfaces. 2013;5(20):10201–6.
[10] Wu L, Li L, Li B, Zhang J, Wang A. Magnetic, durable, and superhydrophobic polyurethane@Fe_3O_4@SiO_2@fluoropolymer sponges for selective oil absorption and oil/water separation. ACS Appl Mater Interfaces. 2015;7(8):4936–46.
[11] Kim D, Kim DW, Buyukcakir O, Kim MK, Polychronopoulou K, Coskun A. Highly hydrophobic ZIF-8/carbon nitride foam with hierarchical porosity for oil capture and chemical fixation of CO_2. Adv Funct Mater. 2017;27(23):1700706.
[12] Du X, Gao B, Li Y, Song Z. Super-robust and anti-corrosive NiCrN hydrophobic coating fabricated by multi-arc ion plating. Appl Surf Sci. 2020;511:145653.
[13] Berger S, Ionov L, Synytska A. Engineering of ultra-hydrophobic functional coatings using controlled aggregation of bicomponent core/shell janus particles. Adv Funct Mater. 2011;21(12):2338–44.
[14] Ren YY, Lin Z, Mao XW, Tian WD, Van Voorhis T, Hatton TA. Superhydrophobic, surfactant-doped, conducting polymers for electrochemically reversible adsorption of organic contaminants. Adv Funct Mater. 2018;28(32):1801466.
[15] Chen S, Fu S, Liang D, Chen X, Mi X, Liu P, et al. Preparation and properties of 3D interconnected CNTs/Cu composites. Nanotechnol Rev. 2020;9(1):146–54.
[16] Wang H, Nie S, Li H, Ali R, Fu J, Xiong H, et al. 3D hollow quasi-graphite capsules/polyaniline hybrid with a high performance for room-temperature ammonia gas sensors. ACS Sens. 2019;4(9):2343–50.
[17] Jian X, Tian W, Li J, Deng L, Zhou Z, Zhang L, et al. High-temperature oxidation-resistant ZrN0.4B0.6/SiC nanohybrid for enhanced microwave absorption. ACS Appl Mater Interfaces. 2019;11(17):15869–80.
[18] Guo Y, Jian X, Zhang L, Mu C, Yin L, Xie J, et al. Plasma-induced FeSiAl@Al_2O_3@SiO_2 core–shell structure for exceptional microwave absorption and anti-oxidation at high temperature. Chem Eng J. 2020;384:123371.
[19] Zhu Q, Pan Q. Mussel-inspired direct immobilization of nanoparticles and application for oil–water separation. ACS Nano. 2014;8(2):1402–9.
[20] Pan Y, Shi K, Peng C, Wang W, Liu Z, Ji X. Evaluation of hydrophobic polyvinyl-alcohol formaldehyde sponges as absorbents for oil spill. ACS Appl Mater Interfaces. 2014;6(11):8651–9.
[21] Chen X, Liang YN, Tang X-Z, Shen W, Hu X. Additive-free poly (vinylidene fluoride) aerogel for oil/water separation and rapid oil absorption. Chem Eng J. 2017;308:18–26.
[22] Beshkar F, Khojasteh H, Salavati-Niasari M. Recyclable magnetic superhydrophobic straw soot sponge for highly efficient oil/water separation. J Colloid Interface Sci. 2017;497:57–65.
[23] Li R, Chen C, Li J, Xu L, Xiao G, Yan D. A facile approach to superhydrophobic and superoleophilic graphene/polymer aerogels. J Mater Chem A. 2014;2(9):3057–64.
[24] Duan B, Gao H, He M, Zhang L. Hydrophobic modification on surface of chitin sponges for highly effective separation of oil. ACS Appl Mater Interfaces. 2014;6(22):19933–42.
[25] Gibson I, Rosen DW, Stucker B. Additive manufacturing technologies. Switzerland: Springer; 2014.
[26] Frazier WE. Metal additive manufacturing: a review. J Mater Eng Perform. 2014;23(6):1917–28.
[27] Kruth J-P, Froyen L, Van Vaerenbergh J, Mercelis P, Rombouts M, Lauwers B. Selective laser melting of iron-based powder. J Mater Process Technol. 2004;149(1–3):616–22.
[28] Yu T, Li M, Breaux A, Atri M, Obeidat S, Ma C. Experimental and numerical study on residual stress and geometric distortion in powder bed fusion process. J Manuf Proc. 2019;46:214–24.
[29] Khairallah SA, Anderson AT, Rubenchik A, King WE. Laser powder-bed fusion additive manufacturing: physics of

complex melt flow and formation mechanisms of pores, spatter, and denudation zones. Acta Mater. 2016;108:36–45.
[30] Yu T, Hyer H, Sohn Y, Bai Y, Wu D. Structure-property relationship in high strength and lightweight AlSi10Mg microlattices fabricated by selective laser melting. Mater Des. 2019;182:108062.
[31] Aboulkhair NT, Everitt NM, Ashcroft I, Tuck C. Reducing porosity in AlSi10Mg parts processed by selective laser melting. Addit Manuf. 2014;1–4:77–86.
[32] Muhammad M, Masoomi M, Torries B, Shamsaei N, Haghshenas M. Depth-sensing time-dependent response of additively manufactured Ti-6Al-4V alloy. Addit Manuf. 2018;24:37–46.
[33] Gong H, Rafi K, Gu H, Starr T, Stucker B. Analysis of defect generation in Ti–6Al–4V parts made using powder bed fusion additive manufacturing processes. Addit Manuf. 2014;1:87–98.
[34] Yakout M, Elbestawi M, Veldhuis SC. A study of thermal expansion coefficients and microstructure during selective laser melting of Invar 36 and stainless steel 316L. Addit Manuf. 2018;24:405–18.
[35] Harrison NJ, Todd I, Mumtaz K. Reduction of micro-cracking in nickel superalloys processed by selective laser melting: a fundamental alloy design approach. Acta Materialia. 2015;94:59–68.
[36] Yan C, Hao L, Hussein A, Young P, Raymont D. Advanced lightweight 316L stainless steel cellular lattice structures fabricated via selective laser melting. Mater & Des. 2014;55:533–41.
[37] Yan C, Hao L, Hussein A, Bubb SL, Young P, Raymont D. Evaluation of light-weight AlSi10Mg periodic cellular lattice structures fabricated via direct metal laser sintering. J Mater Process Technol. 2014;214(4):856–64.
[38] Rehme O, Emmelmann C, editors. Rapid manufacturing of lattice structures with selective laser melting. Lasers and Applications in Science and Engineering. San Jose, California, United States: International Society for Optics and Photonics; 2006.
[39] Zhang H, Gu D, Ma C, Xia M, Guo M. Surface wettability and superhydrophobic characteristics of Ni-based nanocomposites fabricated by selective laser melting. Appl Surf Sci. 2019;476:151–60.
[40] Kang N, El Mansori M, Guittonneau F, Liao H, Fu Y, Aubry E. Controllable mesostructure, magnetic properties of soft magnetic Fe–Ni–Si by using selective laser melting from nickel coated high silicon steel powder. Appl Surf Sci. 2018;455:736–41.
[41] Arakane S, Mizoshiri M, Sakurai J, Hata S. Direct writing of three-dimensional Cu-based thermal flow sensors using femtosecond laser-induced reduction of CuO nanoparticles. J Micromech Microeng. 2017;27(5):055013.
[42] Wang XJ, Liu JY, Yang LJ, He Y, Wang Y. Nano-sized amorphous carbon covered surface formed by selective laser melting of ink-printed (SLM-IP) copper (Cu) nanoparticles (NPs). Appl Surf Sci. 2018;448:133–7.
[43] Wei JJ, Ping H, Xie JJ, Zou ZY, Wang K, Xie H, et al. Bioprocess-inspired microscale additive manufacturing of multilayered TiO_2/polymer composites with enamel-like structures and high mechanical properties. Adv Funct Mater. 2020;30:1904880.
[44] Kruth J-P, Mercelis P, Van Vaerenbergh J, Froyen L, Rombouts M. Binding mechanisms in selective laser sintering and selective laser melting. Rapid Prototyp J. 2005;11(1):26–36.
[45] Singh S, Sharma VS, Sachdeva A. Progress in selective laser sintering using metallic powders: a review. Mater Sci Technol. 2016;32(8):760–72.
[46] Wang X, Liu J, Wang Y, Fu Y. Fabrication of friction-reducing texture surface by selective laser melting of ink-printed (SLM-IP) copper (Cu) nanoparticles (NPs). Appl Surf Sci. 2017;396:659–64.
[47] Banhart J. Manufacture, characterisation and application of cellular metals and metal foams. Prog Mater Sci. 2001;46(6):559–632.